EFDA–JET–CP(10)08/42

G.T.A. Huysmans, S.J.P. Pamela, M.N.A. Beurskens, M. Becoulet, E. van der Plas
and JET-EFDA contributors

Non-linear MHD Simulations of Natural and Pellet Triggered ELMs

Non-linear MHD Simulations of Natural and Pellet Triggered ELMs

G.T.A. Huysmans[1], S.J.P. Pamela[1], M.N.A. Beurskens[2], M. Becoulet[1], E. van der Plas[1] and JET-EFDA contributors*

JET-EFDA, Culham Science Centre, OX14 3DB, Abingdon, UK

[1]CEA, IRFM, F-13108 Saint Paul-lez-Durance, France
[2]JET-EFDA, Culham Science Centre, OX14 3DB, Abingdon, OXON, UK
** See annex of F. Romanelli et al, "Overview of JET Results", (23rd IAEA Fusion Energy Conference, Daejon, Republic of Korea (2010)).*

Preprint of Paper to be submitted for publication in Proceedings of the 23rd IAEA Fusion Energy Conference, Daejon, Republic of Korea (10th October 2010 - 16th October 2010)

ABSTRACT.
Non-linear MHD simulations of ELMs show features that are in good qualitative agreement with experimental observations. The formation of density filaments are due to the ballooning mode convection wheras the sub-structure in the heat deposition profile on the divertor target is dominated by the magnetic field perturbation of the ballooning instability. A first study of the ELM size as a function of collisionality shows an increasing ELM size with decreasing collisionality but only in the 'ideal' MHD regime. The increased losses at lower collisionality are due to the larger parallel heat conduction: the change in the temperature profile increases whereas the convected density losses do not vary with decreasing collisionality.

MHD simulations of pellets 'injected' in an H-mode pedestal can lead to the destabilisation of a ballooning mode due to the high pressure in the pellet cloud for pellet larger than a critical pellet size. In x-point plasmas, the nonlinear MHD simulations indicate a partial direct loss of the pellet density when the pellet cloud arrives at the xpoint. This results in a single spiral in the target heat deposition profile, similar to what has been observed in JET experiments. This structure expands in the toroidal direction with the pellet cloud expanding with the local sound speed.

1. INTRODUCTION

Edge localised Modes (ELMs) are a characteristic feature of the H-mode plasma regime, the standard operation scenario in ITER. ELMs are understood to be MHD instabilities (ballooning modes) destabilised by the large pressure in the H-mode edge pedestal [1-6]. The instability causes energy losses on a fast MHD timescale leading to large energy fluxes to the plasma facing components.

The current estimate of the ELM induced energy losses in ITER results from an extrapolation of the energy losses due to ELMs from current machines towards ITER, based on the experimentally observed scaling of the ELM size with the plasma collisionality [7]. There is as yet no firm explanation of the observed scaling neither theoretical nor from numerical simulations. One important open question is which physical mechanisms and parameters determine the ELM size, i.e. the ELM induced energy losses. The predicted ELM size in ITER is such that the ELMs would lead to an enhanced erosion of the plasma facing components. As a consequence the ELM size in ITER will need to be controlled. One option is to significantly increase the natural ELM frequency by an external trigger. The injection of pellets into the H-mode pedestal has been shown to trigger an ELM or ELM like event at each injected pellet [8-9]. At a large enough pellet frequency, this leads to a synchronisation of the ELMs to the pellet injection frequency. The origin of the trigger of the ELM due to a pellet is still largely unknown.

Non-linear MHD simulations of ELMs can contribute to clarify the physics of ELMs (the onset, amplitude, energy fluxes) and ELM control methods and contribute to an interpretation of the detailed experimental observations of ELMs. In this paper, results are presented on the non linear MHD simulation of ELMs and of pellets, modelled as a large density source, injected in the H-mode pedestal.

2. NON-LINEAR MHD SIMULATION CODE JOREK

The non-linear MHD simulations of ELMs and pellets described below have been obtained with the non-linear MHD code JOREK. In the JOREK code, both the physics variables and the (R,Z) coordinates of the poloidal plane are discretised by so-called (isoparametric) cubic Bezier finite elements [10]. The discretisation leads to a continuous representation of the variables and their derivatives (energy fluxes). The finite element grid in the poloidal plane is aligned with the equilibrium flux surfaces, both inside the separatrix on the closed field lines as on the open field lines. This allows an accurate treatment of the strong anisotropy perpendicular and parallel to the magnetic field. The toroidal variation is described by a Fourier series.

The time advance is using a fully implicit scheme (linearised Crank-Nicholson) on all equations and all variables in one single step. The resulting sparse system of equations is solved using a GMRES iterative solver. As a preconditioner, the sub-matrices of each of the toroidal harmonics are solved using the direct parallel sparse matrix solver PaStiX [11].

Both the full MHD model and reduced MHD models are available in JOREK. For the study presented here, the following reduced MHD model has been applied. The velocity and magnetic field are represented with the ansatz: $\vec{B} = (F_0/R)\,\vec{e_\varphi} + (1/R)\,\vec{\nabla}\psi(t) \times \vec{e_\varphi}$ and $\vec{v} = -R\vec{\nabla}u(t) \times \vec{e_\varphi} + v_{\parallel}(t)\vec{B}$. Inserting this in the usual visco-resistive MHD equations yields the reduced MHD equations for the density, temperature, poloidal flux, electric potential and the parallel velocity (equivalent to [12]), in toroidal geometry. Time (as shown in the figures) is normalised to $\tilde{t} = t/\tau_N$ with $\tau_N = \sqrt{\mu_0 m_D n_D}$.

The boundary conditions on the boundary parallel to the magnetic flux surfaces are Dirichlet conditions, all perturbations to the equilibrium are zero. On the open field lines the parallel velocity is set to Mach one (corresponding to the Bohm condition). The temperature and density have free flow boundary conditions.

3. NON LINEAR MHD SIMULATION OF ELMS

ELMs are generally thought to be due to ballooning (or peeling ballooning) modes which are destabilised by the large pressure gradient (and edge current density) in the H-mode edge pedestal. The evidence for this model for the ELMs is mostly based on the good agreement between the measured pedestal pressure gradient and the calculated linear MHD stability limits [1-6]. Nonlinear MHD simulations are necessary to be able to characterise the consequences of a ballooning instability and compare these with the detailed experimental observations on ELMs that are now available.

Due to the difference in time scales between the slow equilibrium evolution and the fast time scales of an ELM (~200μs), non-linear MHD simulations of ELMs typically start from a ballooning mode unstable equilibrium. The initial equilibria are defined by the choice of the flux at the domain of the computational domain and the density, temperature and current profile as a function of the poloidal flux. The data are either chosen to be "JET-like" equilibria or, more recently, accurately reproducing a time slice from a well-diagnosed JET discharge (Pulse No: 73569) [13].

The initial static solution of the Grad-Shafranov equation is evolved non-linearly (for several

hundred Alfven times) to obtain a quasi-stationary axi-symmetric equilibrium with selfconsistent flows. Figure 1 shows the resulting amplitude of the poloidal flow for JET Pulse No: 73569. The poloidal flow is driven by the pedestal pressure gradient in the presence of dissipative terms (resistivity, diffusivity) amplified by the presence of an x-point [14, 15, 16]. The poloidal flows can be large enough to cause a significant reduction of the ballooning mode growth rates, especially for the higher toroidal mode numbers. The poloidal equilibrium flow also has an influence the non-linear evolution [14,15]. The flow in the parallel direction is predominantly caused by the Bohm boundary conditions at the divertor target.

The non-linear evolution of the ballooning modes shows two very characteristic features: the formation of density filaments and a fine structure in the radial profile of the heat deposition on the target. These features are qualitatively in good agreement with the experimental observations. Figure 2 shows the filaments and the density and temperature profiles of an ELM simulation in a JET-like equilibrium ($R_0 = 3.1$, $B_0 = 2.9$, $q_{99} = 2.8$, $\beta_N = 1.1$, pedestal-width $\delta = 4$cm) at the time of the maximum of the perturbation [17]. The simulation includes the toroidal harmonics $n = 0 - 21$ with a periodicity 3. (Other parameters are resistivity $\eta\,(0) = 5\times10^{-6}$, viscosity $\nu_\perp = 10^{-5}$, diffusivity $D_\perp = 5\times10^{-6}$, $\kappa_\perp = 5\times10^{-6}$, $\kappa_\parallel = 10$)

Filaments are formed due to the flow pattern (vortices) of the predominantly $n = 9$ ballooning mode. The interchange type mode moves high density plasma outwards (in the form of field aligned filaments) and low density "holes" inwards. This creates the characteristic perturbation to the density profile with a local minimum in the density behind the outward moving density filament as measured during ELMs by the high resolution Thomson scattering in MAST [18] and JET [19]. The ballooning mode itself induces an additional $n = 0$ flow which can be in the same direction or opposite to the equilibrium poloidal flow and change direction during the ELM evolution. The $n = 0$ flow is shearing the filaments from the main plasma and limits the amplitude of the filaments. Immediately after the shearing-off of the first set of filaments, there may be several additional bursts of filaments leaving the plasma. This results in a bursty behavior of the density and energy losses. Figure 2 (b) shows the loss rate of density and energy through the separatrix as a function of time during the ELM simulation.

In addition to the flow, the ballooning mode also creates a large magnetic perturbation. The perturbation is large enough to cause a significant ergodisation of the plasma edge in an area of 2-3 times the pedestal width. Figure 3(b) shows a Poincare plot of field lines which have been traced from within the (unperturbed) separatrix. It shows the formation of very thin radially extended structures around the x-point becoming broader further away from the x-point. These structures are characteristic of so-called homoclinic tangles [21,22].

Due to the large parallel conduction, the temperature is close to constant on a magnetic field line. As a consequence the perturbed temperature profile during the ELM closely resembles the structure of the magnetic field perturbations due to the ballooning modes. This results in a fine structure in the temperature at the divertor target forming spirals in the toroidal direction (Fig.3a).

The structures in the temperature translate to structures in the heat convected along the field lines to the target. The radial width of these structures in the JET-like simulations is 1-2cm, agreeing qualitatively with the experimentally observed structures [23-25].

3.1. ELM SIZE SCALING

The most robust scaling of the amplitude of the ELM energy losses as observed experimentally is the scaling of the ELM size with the collisionality ν^* [7]. To try to identify the influence of the collisionality on the ELM size in non linear MHD simulations, the ELM simulations are repeated while varying the density. Since the equations are normalized with respect to the density, the starting static equilibrium remains unchanged and only the coefficients such as the resisivity, diffusivity, conductivity and viscosity will change with collisionality. The parallel heat conduction $\parallel$ has the strongest collisionality dependence, $\kappa_{\parallel} \sim 1/\nu^*$, the other coefficients scale as $\nu^{*-1/6}$. Note that this scan is not at constant ρ^*. The starting equilibrium is JET Pulse No: 73569, reconstructed from the electron pressure profile just before the ELM onset using the (coherent ELM average) HRTS profiles [19], the EFIT current density profile to which the edge bootstrap current has been added and the poloidal flux on a contour close to the JET vessel. These simulations have been done using the reduced MHD model with ion and electron temperatures, at very high poloidal resolution (with up to 22000 cubic finite elements) while using one single toroidal harmonic (in addition to n = 0) at the time.

Figure 4 shows the collisionality dependence of the growth rates and the ELM size for the JET equilibrium and a resistivity of $\eta = 10^{-7}$ at $\nu^* = 1$. The ELM size scaling in this case is opposite to the experimental scaling. This is due to the dependence of the mode growth rates on the resistivity (the equilibrium is only marginally unstable to ideal MHD ballooning modes). In order to investigate the regime where the ballooning instability is closer to the ideal MHD regime, the edge pressure gradient is (artificially) increased by 50% (by reducing the pedestal width) and by choosing a resistivity of $\eta = 10^{-8}$ at $\nu^* = 1$. In this 'ideal' regime,the growth rates do not show a strong dependence on the collisionality. The scaling of the ELM size with collisionality now has the same trend as in experiment. The increase of the ELM energy losses with collisionality in these simulations is mainly due to the increasing parallel conduction losses with decreasing collisionality. This is also reflected in the scaling of the density and temperature losses (Fig.4). The relative density losses do not show a dependence whereas the relative temperature losses increase at lower collisionality [13].This trend is similar to the experimental observations [19]. The importance of parallel conduction losses has been discussed for example with respect to ELMs in JET [19] and in theoretical ELM models [20].

An additional scaling can be expected from the collisionality dependence of the most unstable mode number and the dependence of the bootstrap current which have not been taken into account in this initial study. Note that the ELM size dependence does not yet consider the full ELM cycle. It does include the ELM relaxation from a given unstable state to a relaxed state. For a complete ELM cycle several consecutive ELMs will need to be simulated. This is a formidable numerical challenge due to the different time scales involved.

4. NON LINEAR MHD SIMULATION OF PELLETS IN THE H-MODE PEDESTAL

The injection of pellets into the H-mode pedestal is one of the methods of ELM control foreseen in ITER. Experimentally, it is observed that pellets trigger an ELM or ELM-like event when injected in the H-mode pedestal. The ELM can be triggered in any phase of a natural ELM cycle (except immediately after a natural ELM). Injection of a pellet in Ohmic, L-mode and QH-mode plasmas also yields a (smaller) magnetic perturbation but not an ELM-like event [26]. In AUG it was shown that the ELM is triggered when the pellet reaches the middle of the transport barrier, independent of the velocity and mass of the pellet [27]. The cause for the trigger is still largely unknown.

To study the possible causes for the pellet trigger of an ELM or ELM-like event, the evolution of the H-mode plasma with an injected pellet is simulated with the non-linear MHD code JOREK. The pellets are modelled as a large localised (non-moving) density source localised in the middle of the H-mode pedestal. The consequence of the large (adiabatic) density source is a strong increase in the local density and a local cooling of the temperature at the position of the density source. Due to the large parallel heat conduction, the temperature is partially restored leading to an increase in the pressure in the pellet cloud. This increase in pressure drives the parallel convection which spreads the density perturbation along the magnetic field with the local sound speed.

The influence of the amplitude of the pellet source and its position (low-field or high field side) on the possible trigger of a ballooning-like instability has been studied, first in circular plasmas [28]. The initial equilibria ($R = 3.0$m, $a = 0.92$m , $B_0 = 3.0$T, $I = 1.6$MA , $\beta_p = 0.6$) are characterized by a large pressure gradient at the edge, representing the H-mode edge pedestal. The equilibrium is marginally stable to ballooning modes with toroidal mode numbers used in the simulation ($n = 0–15$). The pellet is represented by a particle source at mid-pedestal (at $q = 2.2$) with a horizontal, vertical and toroidal width of 3cm by 23cm by 70 degrees resp.

The source amplitude has been varied from $S = 2.1\times10^{23}$ s^{-1} to $S = 2.1\times10^{24}$ s^{-1} (assuming a central density of 5×10^{19} m^{-3}). The central resistivity used in the simulations is $\eta = 5\times10^{-8}$, the ratio of the parallel to perpendicular heat conduction is $\kappa_{\parallel} / \kappa_{\perp} = 2.5\times10^{7}$. The grid size is defined by 51 radial cubic C^1 finite elements, strongly packed around the pellet position, and 128 poloidal elements. At $S = 2.1\times10^{24}$ s^{-1} the pressure and density at the source build up in typically $10\tau_N$ ($\tau_N = \sqrt{\mu_0 m_0 n_0}$ at $n_D = 5\times10^{19}$ m^{-3}, $\tau_N = 4.6\times10^{-7}$ s), after which they remain relatively constant. The maximum density increases locally by a factor ~7 and the pressure by a factor ~5. On the same time scale, there is fast increase of the low-n toroidal harmonics.

The plasma response to the pellet consists of two phases. The initial response scales linearly with the amplitude of the pellet source. This response is most likely due to the loss of equilibrium due to the pressure perturbation. The induced electric field leads to the wellknown E × B drift of the pellet. Figure 5a shows the evolution of the kinetic energy for the modes $n = 8–15$ for 3 values of the pellet amplitude 'injected' on the low-field side.

For large enough pellets, a ballooning type instability develops in addition to the linear response. On the low-field side the instability deforms the pellet cloud into a filamentary structure moving

outwards. The pellet cloud remains unstable when it has expanded to the high-field side after $2\pi R/c_s \sim 100\tau_N$. On this side, the instability develops on the inside of the pellet cloud where the pellet pressure gradient is destabilising in the good curvature region. Here, the ballooning instability develops fingers inwards. Figure 5 shows the density and flow contours for a large unstable pellet cloud compared to a smaller stable case. The critical amplitude above which the ballooning instability develops is $S < 1\times10^{24}\ s^{-1}$. The cause for destabilization is the high pressure inside the high density plasmoid and the associated local increase of the pressure gradient. The local cooling of the plasma due to the density source leading to an increase in the resistivity will also contribute to the destabilization.

For a pellet source on the high field side at mid-pedestal the behavior is globally very similar to the low field side pellets. Also in this case a ballooning mode can develop for large enough pellets (see Fig.6). The instability develops first at the high field side plasmoid before the density perturbation has reached the low field side. This leads to density filaments being injected further into the plasma (see close up in Figure 6, right). Only when the density perturbation reaches the low field are density filaments moving out of the plasma. The critical amplitude for the onset of the ballooning instability is very similar for high field side and low field side pellets.

The evolution of the plasma response to a 'pellet' (a large localized density source) in a JETlike H-mode plasma at mid-pedestal ($R_0 = 3.1$m, $a = 0.89$m, $B = 2.9$T, $I = 3.2$MA , $\beta_N = 1.0$) is qualitatively the same as in described above for circular plasmas. The pedestal pressure is chosen such that it is marginally stable to ballooning modes (for the mode numbers (n = 0-15) and the resistivity, $\eta = \times10^{-8}$, used in the simulation). Figure 7(a) shows the density contour, at the density on axis, of the pellet cloud at $t = 217\tau_N$ after the start of the pellet source at a source rate of $S < 1\times10^{24}\ s^{-1}$ in the outer mid-plane. At this time the number of ions has increased by 3.8%. At this large source rate, there is a ballooning-like instability developing with a (predominantly) single helical perturbation consisting of many coupled toroidal harmonics. The simulations are not advanced to the point where (possibly) a filament is ejected from the plasma.

The heat flux convected to the target during the pellet evolution shows the formation of toroidally localized heat flux (after about $130\,\tau_N$ after the start of the pellet) at the position where the density (and temperature) perturbation reaches the x-point (see Fig.7(b)). At the xpoint, the density flows across the separatrix onto the outer target. These 'prompt' density losses lead to a spiral structure in the heat flux with one 'stripe' in addition to the normal strike-point. This structure is qualitatively very similar to the structure in heat deposition profile with a single additional maximum observed during the JET pellet triggered ELMs [29]. In the MHD simulations this additional peak in the heat flux extends in the toroidal direction on a time scale of $100\,\tau_N$ (approx. the local sound speed) to cover almost ¾ of the toroidal circumference. At this time most of the additional heat flux occurs at the original strike-point. In contrast to the ELM simulations, the magnetic perturbation does not cause a large ergodisation. There is an ergodic layer of about 2cm inside the separatrix but no large structures due to homoclinic tangles as in the ELM simulations. The single spiral in the target

heat deposition is due to density convected through the x-point and is not (as in the case of natural ELMs) directly related to the magnetic perturbation.

CONCLUSIONS

A first study of the ELM size in non-linear MHD simulations shows an increasing ELM size with decreasing collisionality in the 'ideal' MHD regime (albeit with a weaker dependence). The heat conduction parallel to the ergodised magnetic field appears to be the dominant effect leading to larger temperature losses at constant density losses with decreasing collisionality. The pressure in the pellet cloud in the H-mode pedestal can trigger a ballooning instability leading to an initially single helical perturbation consisting of many toroidal harmonics. The non-linear MHD simulations show partial prompt density losses of the pellet cloud when arriving at the x-point. This leads to an additional spiral structure in the heat deposition profile on the target similar to the structures observed in the JET pellet injection experiments.

ACKNOWLEDGEMENT

This work, supported by the European Communities under the contract of Association between EURATOM and CEA, was carried out within the framework of the European Fusion Development Agreement. The views and opinions expressed herein do not necessarily reflect those of the European Commission. This work, as part of the project ANR-CIS2006.001, has benefitted from financial support from the 'Agence National de Recherche'. Discussions with R. Wenninger, G. Kocsis and P. Lang are gratefully acknowledged.

REFERENCES

[1]. P. Snyder et al., Physics of Plasmas **9**, 2037, (2002)
[2]. P. Snyder et al., Nuclear Fusion **49** 085035 (2009)
[3]. S. Saarelma, et al., Plasma Physics and Controlled Fusion **49**, 31, (2007)
[4]. S. Saarelma, et al., Plasma Physics and Controlled Fusion **51**, 035001 (2009)
[5]. H.R. Wilson et al, Plasma Physics and Controlled Fusion **48** A71 (2006)
[6]. G.T.A. Huysmans, Plasma Physics and Controlled Fusion **47**, B165 (2005)
[7]. A Loarte et al., Plasma Physics and Controlled Fusion **45** 1549 (2003)
[8]. P.T. Lang et al., Nuclear Fusion **43** 1110–1120 (2003)
[9]. P.T. Lang et al., Nuclear Fusion **47** 754 (2007)
[10]. O. Czarny and G. Huysmans, J. Comp. Phys., Volume 227 ,Issue 16, (2008) p. 7423-7445
[11]. P. Henon et al., Parallel Computing, **34**:345-362, 2008
[12]. H.R. Strauss, Journal ofPlasma Physics, vol. **57**, part 1, (1997) pp. 83-87
[13]. S. Pamela et al., 37th EPS conference on Plasma Physics, Dublin (2010)
[14]. S. Pamela et al., Plasma Physics and Controlled Fusion **52** 075006 (2010)
[15]. A.Y. Aydemir, Physics of Plasmas **14**, 056118 (2007)

[16]. H.R. Strauss, Physics of Plasmas **2** 1229 (1995)
[17]. G.T.A. Huysmans, Plasma Physics and Controlled Fusion **51** 124012 (2009)
[18]. A. Kirk et al., PRL 96, 185001 (2006)
[19]. M.N.A. Beurskens et al., Nuclear Fusion **49** (2009) 125006 (13pp)
[20]. W. Fundamenski et al., Plasma Physics and Controlled Fusion **48** (2006) 109–156
[21]. T.E. Evans et al., J. Phys.: Conf. Ser. 7 174 (2005)
[22]. L.E. Sugiyama and H.R. Strauss, Phys. Plasmas **17**, 062505 (2010)
[23]. T. Eich et al., Physics Revie Letters **91**, 195003 (2003)
[24]. T. Eich et al., Plasma Physics and Controlled Fusion **47** (2005) 815–842
[25]. S. Devaux, 36th EPS conference on Plasma Physics, Sofia (2009)
[26]. P.T. Lang et al., Nuclear Fusion **48** 1-12 (2008)
[27]. G. Kocsis et al., Nuclear Fusion **47** 1166-1175 (2007)
[28]. G.T.A. Huysmans, 37th EPS conference on Plasma Physics, Dublin (2010)
[29]. R. Wenninger et al., 37th EPS conference on Plasma Physics, Dublin (2010)

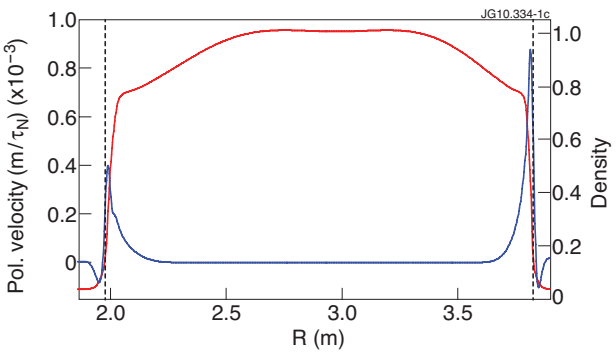

Figure 1: Equilibrium poloidal flow (blue) in MHD simulation of JET discharge

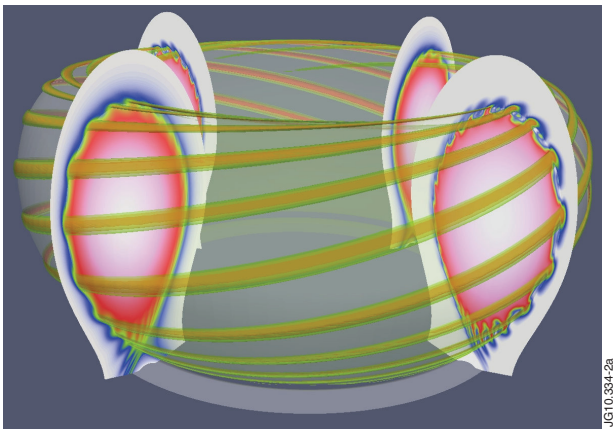

Figure 2(a): The density (right) and temperature (left) profiles together with the density filaments outside the separatrix.

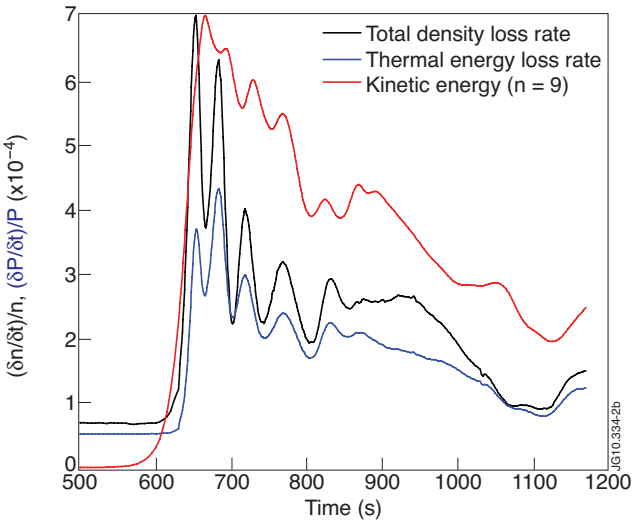

Figure 2(b): The time evolution of the relative loss rate of the total density and total thermal energy inside the separatrix (in units of τ_N).and the kinetic energy of the dominant n = 9 mode.

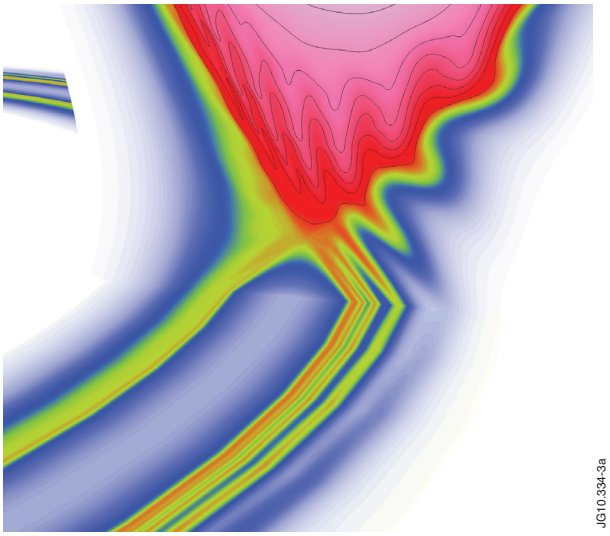

Figure 3(a): Temperature in a poloidal plane and at the divertor target at the time of maximum ELM amplitude.

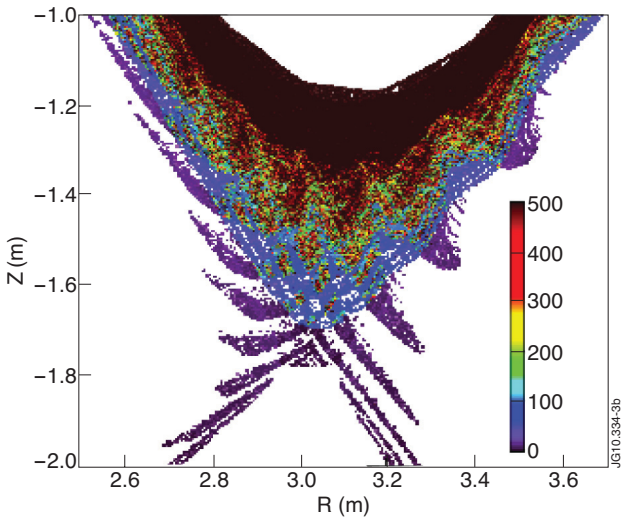

Figure 3(b):Poincare plot of field lines starting inside the (unperturbed) separatrix. Color indicates the connection length.

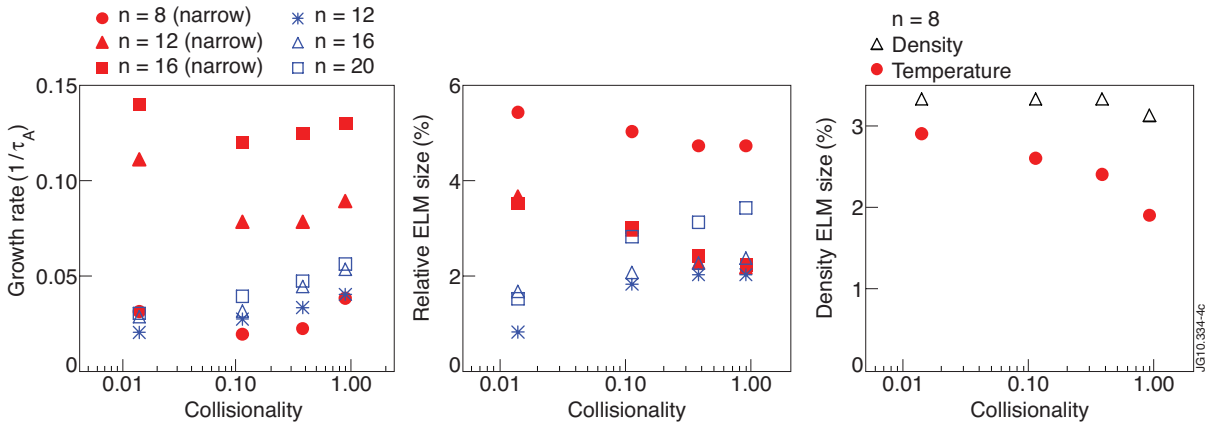

Figure 4: The collisionality dependence of the growth rate (left), the relative ELM size (middle) and the relative density and temperature losses (right) for the original JET simulation (blue, open symbols) and the simulation with increased edge pressure gradient (red, closed symbols).

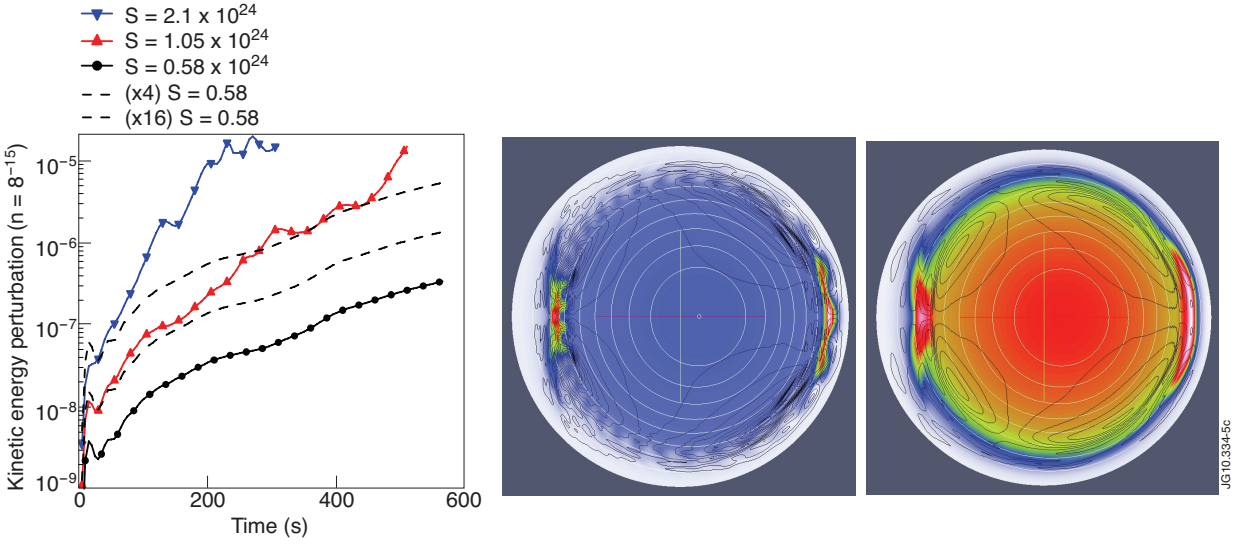

Figure 5: The evolution of the kinetic energy of the harmonics n=8-15 as a function of the pellet size (particle source) for pellets at the low-field side mid plane. The density and flow contours for the source rate $S = 2.1 \times 10^{24}\ s^{-1}$ (middle) and $S = 0.57 \times 10^{24}\ s^{-1}$ (right).

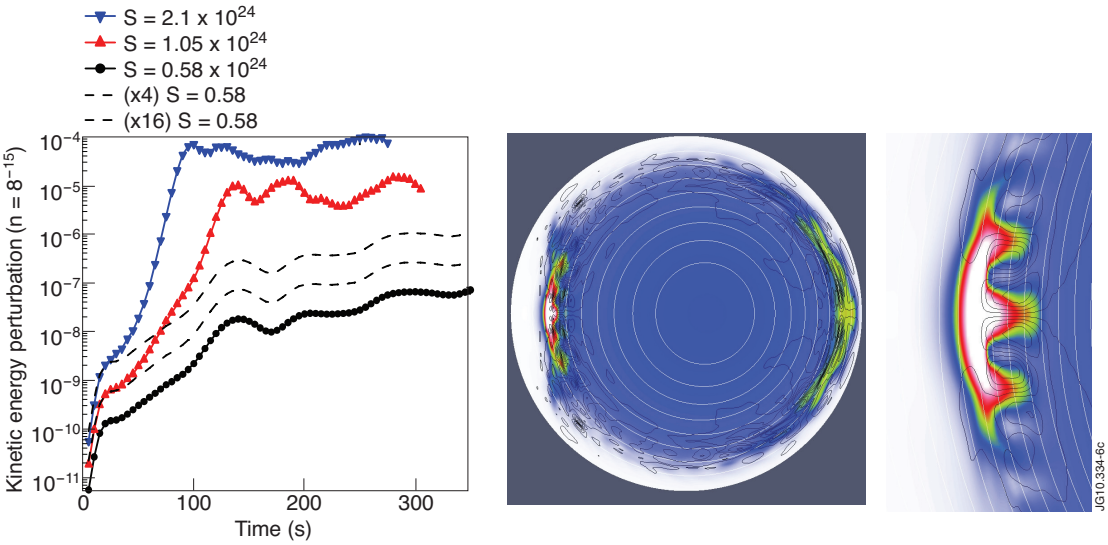

Figure 6: The evolution of the kinetic energy of the harmonics n=8-15 as a function of the pellet size (particle source) for pellets at he high field side mid plane. The density and flow contours for the source rate S = 2.1 × 10^{24} s^{-1} (middle) at t = 250τ_N with a close-up view of the high field side pellet cloud (right).

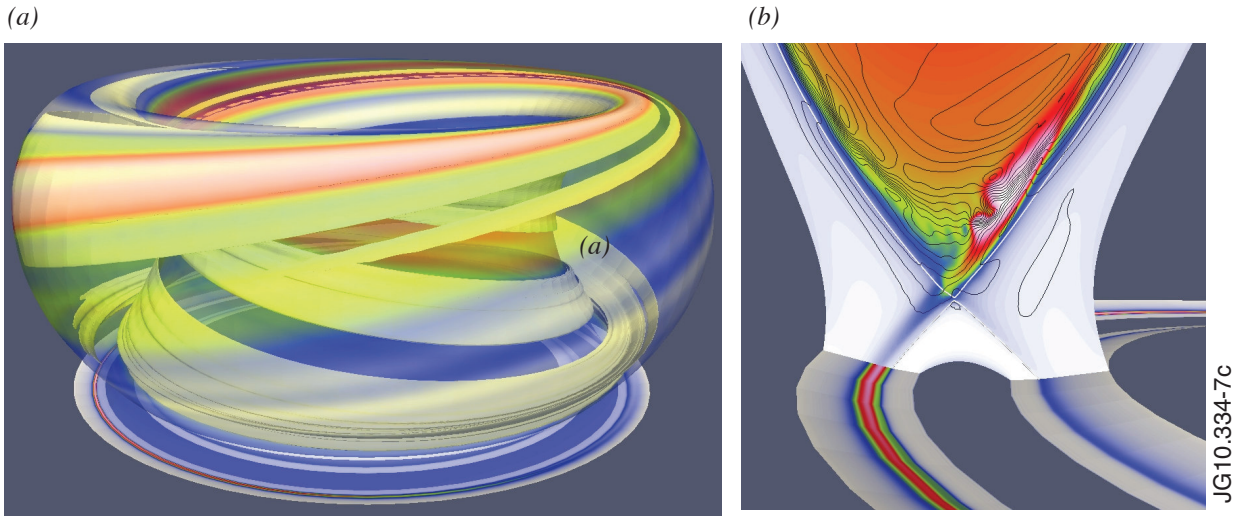

Figure 7(a): Density contour (central density, yellow) during pellet injection and the temperature on the (unperturbed) separatrix after 217τ_N with 3.8% additional particles injected. Temperature on the separatrix (blue-red scale).
Figure 7b): Density (color) and flow lines showing the prompt losses of density at the x-point causing a spiral in the convected heat flux at the target.